Macromolecules

Article

pubs.acs.org/Macromolecules

Relationship of Extensional Viscosity and Liquid Crystalline Transition to Length Distribution in Carbon Nanotube Solutions

Dmitri E. Tsentalovich,[†] Anson W. K. Ma,[†,‡] J. Alex Lee,[†] Natnael Behabtu,[†] E. Amram Bengio,[†] April Choi,[†] Junli Hao,[†] Yimin Luo,[†] Robert J. Headrick,[†] Micah J. Green,[§] Yeshayahu Talmon,[∥] and Matteo Pasquali*[,†]

[†]Department of Chemical & Biomolecular Engineering, Department of Chemistry, Department of Materials Science & NanoEngineering, The Smalley Institute for Nanoscale Science & Technology, Rice University, Houston, Texas 77005, United States

[‡]Department of Chemical & Biomolecular Engineering, University of Connecticut, Storrs, Connecticut 06269, United States

[§]Artie McFerrin Department of Chemical Engineering, Texas A&M University, College Station, Texas 77843, United States

[∥]Department of Chemical Engineering, Technion-Israel Institute of Technology and The Russell Berrie Nanotechnology Institute (RBNI), Haifa 3200003, Israel

Supporting Information

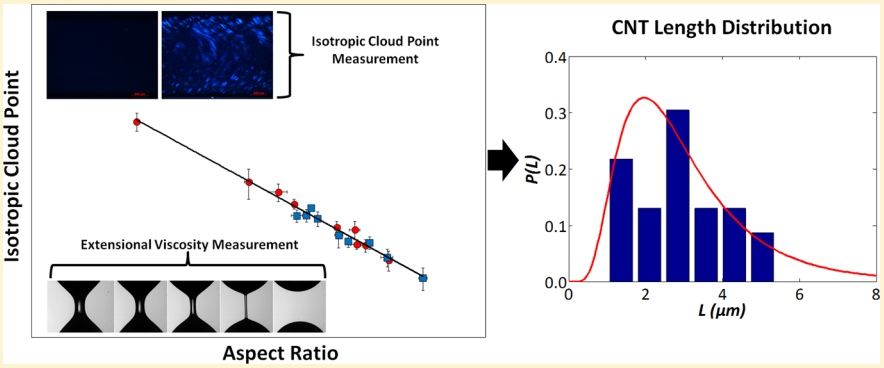

ABSTRACT: We demonstrate that the length of carbon nanotubes (CNTs) can be determined simply and accurately from extensional viscosity measurements of semidilute CNT solutions. The method is based on measuring the extensional viscosity of CNT solutions in chlorosulfonic acid with a customized capillary thinning rheometer and determining CNT aspect ratio from the theoretical relation between extensional viscosity and aspect ratio in semidilute solutions of rigid rods. We measure CNT diameter d by transmission electron microscopy (TEM) and arrive at CNT length L. By studying samples grown by different methods, we show that the method works well for CNT lengths ranging from 0.4 to at least 20 μm, a wider range than for previous techniques. Moreover, we measure the isotropic-to-nematic transition concentration (i.e., isotropic cloud point) φ_{iso} of CNT solutions and show that this transition follows Onsager-like scaling $\varphi_{iso} \sim d/L$. We characterize the length distributions of CNT samples by combining the measurements of extensional viscosity and transition concentration and show that the resulting length distributions closely match distributions obtained by cryo-TEM measurements. Interestingly, CNTs appear to have relatively low polydispersity compared to polymers and high polydispersity compared to colloidal particles.

Carbon nanotubes (CNTs) are perhaps the ultimate class of polymers.[1] At the molecular scale, they display exceptional mechanical strength and electrical and thermal conductivity.[2,3] This unique combination of properties makes CNTs promising for biomedical, consumer electronics, and industrial applications, e.g., sensory fibers,[4] touch screens,[5−7] field emission tips,[8] and multifunctional cables.[9] Even though the properties of macroscopic CNT assemblies still fall short of their exceptional single molecule values, macroscopic CNT fibers already display a record combination of mechanical and transport properties,[9] while CNT films and coatings are being used for transparent conductive electrodes[10] and electromagnetic interference shielding.[11]

In CNT fibers and films, the main hurdles to attaining the desired properties include difficult processing and insufficient CNT length and quality. Theoretical calculations and experimental evidence indicate that fiber strength scales with CNT aspect ratio[9,12−14] and that fiber and film conductivity[5,9,15] scale with CNT length.

Theory also predicts that the isotropic cloud point φ_{iso}, i.e., the transition concentration of CNTs in solution from an isotropic to a nematic liquid crystalline phase, scales with CNT

Received: September 16, 2015
Revised: December 16, 2015
Published: January 6, 2016

DOI: 10.1021/acs.macromol.5b02054
Macromolecules 2016, 49, 681−689

aspect ratio.[16] While experiments have studied how this transition concentration depends on solvent quality,[17] up to now the effect of aspect ratio on CNT liquid crystalline phase behavior has not been studied experimentally. Studying this effect is important for developing both fundamental understanding and engineering technology for processing of CNT solutions, yet such a study requires accurate measurements of CNT length.

Despite the importance of accurate CNT length determination, existing measurement methods have limited reliability and can be applied only in restricted length ranges.[18] These methods include atomic force microscopy (AFM),[19,20] cryogenic-temperature transmission electron microscopy (cryo-TEM),[21] dynamic light scattering (DLS),[22] length analysis by nanotube diffusion (LAND),[23] scanning electron microscopy (SEM),[24] and shear viscosity.[25] While all of these techniques give a reasonable estimate of CNT length, each has its own drawbacks.

AFM and cryo-TEM rely on small sample size (typically hundreds of CNTs) and have a potential imaging bias toward longer CNTs.[26] Typically, AFM, DLS, and LAND require sonication to ensure complete CNT dispersion, which cuts CNTs and consequently changes their length distribution. Because sonication preferentially cuts the longest CNTs,[27−29] AFM, DLS, and LAND are less accurate for CNT samples with higher average lengths. In addition, LAND is limited to probing semiconducting SWNTs because it is a fluorescence-based method. SEM is not limited to any specific range of CNT lengths, but it cannot be applied to bulk-grown CNTs and is primarily used to measure the length of carpet-grown CNTs, which grow perpendicularly to the substrate; even in the case of carpet-grown CNTs, SEM imaging relies on the underlying assumption of monodisperse length, which may not always be valid.[24]

Shear viscosity can be used to determine the aspect ratio of CNTs more quickly and reliably than AFM or cryo-TEM because it is a bulk measurement that probes ~10^{10} CNTs.[25,30] Moreover, it can be performed on pristine CNTs dissolved in superacids, thereby avoiding sonication.[31] Length determination by shear rheology is based on the relation between the viscosity of a dilute suspension of isotropically oriented rods (i.e., their zero-shear viscosity) and the rods' concentration and aspect ratio. Because shearing aligns rods, which in turn reduces the rods' contribution to the suspension viscosity, the measurements must be carried out at very low shear rates, such that the viscous torque on the rods does not exceed the Brownian torque; in practice, direct rotational diffusivity measurements on individualized CNTs[32] indicate that the shear rheology method is limited to CNTs of lengths below ~1 μm (see section S1 for details).

Here we introduce a length determination method based on extensional viscosity measurement; this method is applicable to a wider range of CNT length than AFM, DLS, LAND, or shear viscosity, while retaining all the advantages of the shear viscosity method. Our work extends the experimental studies that have been performed on CNT extensional rheology[33,34] by determining CNT aspect ratio from extensional viscosity measurements on solutions of CNTs dissolved in chlorosulfonic acid, a true thermodynamic solvent for CNTs.[17,35] CNT length is determined by combining the aspect ratio measurements with the average CNT diameter measured by TEM. We also study the dependence of the isotropic cloud point on aspect ratio and combine these data with our length measurements to fully characterize the length distributions of CNT samples produced by various manufacturers.

THEORETICAL BASIS

When a liquid drop is stretched into a filament beyond a critical threshold, the capillary pressure at the mid-filament pumps the liquid toward the filament's ends, inducing a strong extensional flow.[36,37] The filament thinning dynamics are controlled by the balance of surface tension, inertia, gravity, and viscosity. Inertia is negligible when viscous forces are dominant over inertial forces (i.e., when the Ohnesorge number $Oh > 1$). For semidilute CNT solutions in chlorosulfonic acid, the Ohnesorge number is

$$Oh = \frac{\eta_0}{\sqrt{\rho_s \frac{D_0}{2}\gamma}} \approx \frac{(1\ \text{Pa s})}{\sqrt{\left(1750\frac{\text{kg}}{\text{m}^3}\right)(0.6\ \text{mm})\left(38\frac{\text{mN}}{\text{m}}\right)}} = 5 \quad (1)$$

where ρ_s is the solvent density, D_0 is the initial filament diameter, γ is the surface tension, and η_0 is the zero-shear viscosity. The effects of gravity are negligible when the Bond number Bo, which represents the ratio of gravitational to surface tension forces, is small (e.g., $Bo \ll 1$). This is the case for our experiments, for which the Bond number is

$$Bo = \frac{\rho_s D_0^{\,2} g}{4\gamma} = \frac{\left(1750\frac{\text{kg}}{\text{m}^3}\right)(1.2\ \text{mm})^2\left(9.8\frac{\text{m}}{\text{s}^2}\right)}{4\left(38\frac{\text{mN}}{\text{m}}\right)} = 0.16 \quad (2)$$

where g is the gravitational acceleration.

If the surface tension is known, the extensional viscosity can be determined by monitoring the time evolution of the filament midpoint diameter.[38] Like in shear flow, rods align in extensional flow when the viscous torque exceeds the Brownian torque (Figure 1). Unlike in shear, the rods' contribution η_r to

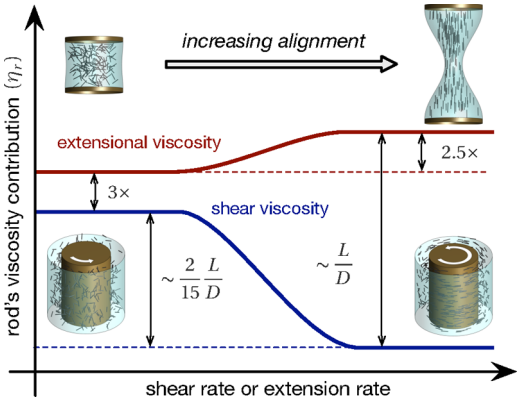

Figure 1. Schematic showing that rods in dilute and semidilute solutions align with increasing shear and extension rate (Peclet or Weissenberg number). Relative increases in η_r for the low and high shear/extension rate limits are indicated on the plot.

the suspension viscosity grows as the rods become aligned (Figure 1) and reaches a plateau whose value is determined by the rods' concentration and aspect ratio.[39,40] Therefore, length measurement by extensional viscosity does not suffer from an intrinsic limitation on rods length. Moreover, it is expected to be more accurate in systems of longer rods, where alignment can be induced readily by flow. Thus, such a length

DOI: 10.1021/acs.macromol.5b02054
Macromolecules 2016, 49, 681−689

measurement method is appropriate in principle for measuring the length of CNTs dissolved in chlorosulfonic acid, which behave as rigid rods in a true solvent.[41]

The uniaxial extensional viscosity η_E is defined as the difference of the axial $\boldsymbol{\tau}_{zz}$ and radial $\boldsymbol{\tau}_{rr}$ normal stresses divided by the extensional strain rate $\dot{\epsilon}$

$$\eta_E = \frac{\boldsymbol{\tau}_{zz} - \boldsymbol{\tau}_{rr}}{\dot{\epsilon}} \tag{3}$$

The difference of the normal stresses can be approximated from a force balance on a thinning filament by lumping the effects of inertia, gravity, and axial curvature into an effective parameter X.[38] By approximating $\dot{\epsilon}$ as the midplane extension rate[42,43] $\dot{\epsilon}_{mid}$ based on the decay rate of the midfilament diameter D_{mid}

$$\dot{\epsilon}_{mid} = -\frac{2}{D_{mid}}\frac{dD_{mid}}{dt} \tag{4}$$

where t is time, the apparent extensional viscosity $\eta_{E,app}$ is[44]

$$\eta_E \approx \eta_{E,app} = \frac{(2X-1)\gamma}{-\frac{dD_{mid}}{dt}} \tag{5}$$

Both simulations[45] and experiments[38] show that $X = 0.7127$ is an appropriate value for viscous Newtonian fluid filaments with negligible inertia and smoothly necked profiles. Smoothly necked profiles typically form only toward the later stages of filament thinning for Newtonian fluids.[38] In extension, solutions of fully aligned rods behave as Newtonian fluids; therefore, we use the value $X = 0.7127$ to extract the extensional viscosity from our experiments. Neglecting the effect of Brownian stresses, the total stress $\boldsymbol{\tau}$ in a liquid dispersion of rigid cylindrical rods is[46]

$$\boldsymbol{\tau} = 2\mu\mathbf{D} + \nu\zeta_{str}\langle\mathbf{uuuu}\rangle{:}\mathbf{D} \tag{6}$$

where μ is the solvent viscosity, $\mathbf{D}$ is the strain rate tensor, ν is the number concentration of rods in solution, and $\mathbf{u}$ is a unit vector describing the orientation of a rod. In a semidilute solution of rods, the expression of the viscous drag coefficient ζ_{str} can be derived by extending Bachelor's theory[47] to account for multiparticle hydrodynamic interactions[40]

$$\zeta_{str} = \frac{\pi\mu L^3}{3\left(\ln\left(\frac{1}{\varphi}\right) + \ln\left(\ln\left(\frac{1}{\varphi}\right)\right) + A\right)} \tag{7}$$

where L is rod length, $A = 0.1585$ is the shape parameter for fully aligned rods, and φ is rod volume fraction. Equation 6 assumes that the Brownian contribution to the total stress is negligible. This is true when the rotational Peclet number $Pe \gg 1$, where Pe is defined as

$$Pe = \frac{\dot{\epsilon}_{mid}}{D_r} \tag{8}$$

and the rotational diffusivity D_r for rigid rods is

$$D_r = \frac{k_B T}{2\zeta_{str}} \tag{9}$$

where k_B is Boltzmann's constant and T is temperature. For low CNT volume fraction ($0.005\% < \varphi < 0.5\%$) in chlorosulfonic acid ($\mu = 2.8$ mPa·s) at room temperature, $D_r < 10$ s^{-1} for CNTs longer than ~1 μm (according to eqs 7 and 9). Since the capillary thinning rheometer is operated at initial strain rates of at least 100 s^{-1} to ensure fully aligned CNTs, this means that from eq 8 we get $Pe > 10$ and Brownian stresses are negligible as long as CNTs are ~1 μm or longer. For shorter CNTs, we can still neglect rotational Brownian motion by operating the rheometer at strain rates higher than 100 s^{-1}. However, even for the shortest CNTs that were tested (~0.3 μm average length), there was no statistically significant change in extensional viscosity when the initial step strain rate was increased from 100 to 200 s^{-1}, indicating that an initial strain rate of 100 s^{-1} was high enough for all the samples tested in this work. Assuming that the rods are fully aligned (i.e., $\mathbf{u} = \mathbf{e}_z$ in eq 6, where $\mathbf{e}_z$ is the direction of uniaxial stretching), eqs 3 and 6 yield the uniaxial extensional viscosity

$$\eta_E = 3\mu + \nu\zeta_{str} \tag{10}$$

In a system of cylindrical rods, the number density ν is related to the volume fraction by

$$\nu = \frac{4\varphi}{\pi d^2 L} \tag{11}$$

Equations 7, 10, and 11 yield the dependence of the extensional viscosity on rod aspect ratio for semidilute solutions of fully aligned, length and diameter monodisperse rigid rods

$$\eta_E = 3\mu\left[1 + \frac{4\varphi\left(\frac{L}{d}\right)^2}{9\left[\ln\left(\frac{1}{\varphi}\right) + \ln\left(\ln\left(\frac{1}{\varphi}\right)\right) + 0.1585\right]}\right] \tag{12}$$

However, CNTs are typically polydisperse in both diameter and length. Because CNT diameters vary by less than a factor of 3 for the samples tested in this work, hereafter we consider CNT diameter to be effectively monodisperse. AFM and LAND length measurements indicate that most CNT length distributions are described well by the log-normal distribution,[23,30] for which the probability density function $P(L)$ is

$$P(L) = \frac{1}{LS\sqrt{2\pi}}\exp\left[-\frac{(\ln(L) - m)^2}{2S^2}\right] \tag{13}$$

where m is the mean and S^2 is the variance of the natural logarithm of L. Truncating the log-normal distribution at the shortest and longest lengths of CNTs in solution, the moments of the length distribution are defined over the interval $L_{min} < L < L_{max}$

$$\langle L\rangle = \int_{L_{min}}^{L_{max}} LP(L)\,dL \approx e^{m+(1/2)S^2} \tag{14}$$

$$\langle L^2\rangle = \int_{L_{min}}^{L_{max}} L^2P(L)\,dL \approx \langle L\rangle^2 e^{S^2} \tag{15}$$

$$\langle L^3\rangle = \int_{L_{min}}^{L_{max}} L^3P(L)\,dL \approx \langle L\rangle^3 e^{3S^2} \tag{16}$$

where the approximate equalities are valid in the limit of $L_{min} \to 0$ and $L_{max} \to \infty$. To characterize the length distribution of CNTs from extensional viscosity measurements, a viscosity average length L_v is introduced analogously to the viscosity average molecular weight used to compare molar mass distributions for polymers:[48]

$$L_v = \left[\frac{\langle L^{1+a}\rangle}{\langle L\rangle}\right]^{1/a} \tag{17}$$

DOI: 10.1021/acs.macromol.5b02054
Macromolecules 2016, 49, 681−689

where a is an exponent that relates L to the intrinsic extensional viscosity $[\eta_E]$

$$[\eta_E] \equiv \lim_{\varphi \to 0} \frac{\eta_E - 3\mu}{3\mu\varphi} = \frac{4}{9}\left[\ln\left(\frac{1}{\varphi}\right) + \left(\ln\left(\ln\frac{1}{\varphi}\right)\right) + 0.1585\right]^{-1}\left(\frac{L}{d}\right)^2 \quad (18)$$

from which it is clear that $a = 2$ for solutions of fully aligned rods in a uniaxial extensional flow; thus, L_v is defined in terms of the third and first moments of the length distribution

$$L_v = \sqrt{\frac{\langle L^3\rangle}{\langle L\rangle}} \quad (19)$$

We replace L by L_v in eq 12, so that eq 12 can be applied to length polydisperse samples. Thus, we can extract L_v from extensional viscosity measurements of CNT solutions. Since L_v is a ratio of two moments, an additional measurement is needed to obtain the value of both moments independently.

We obtain the first and third moments by measuring isotropic cloud point, in addition to extensional viscosity. For polydisperse hard rods, the dependence of the isotropic cloud point φ_{iso} on the moments of the rod length distribution has been described by Wensink and Vroege[49]

$$\varphi_{iso}(\sigma_L) = \frac{d}{L_0} c_{iso}(\sigma_L) \quad (20)$$

where L_0 is an arbitrary characteristic length, c_{iso} is the rod number density at the isotropic cloud point for a specific length distribution, and σ_L is a length polydispersity index. We define σ_L analogously to the molecular weight polydispersity index used for polymer samples

$$\sigma_L = \frac{\langle L^2\rangle}{\langle L\rangle^2} \quad (21)$$

Thus, by measuring L_v, φ_{iso}, and d for each CNT sample and using the analysis of Wensink and Vroege,[49] it is possible to determine the statistical parameters of each sample's length distribution.

For the log-normal distribution, the function c_{iso} can only be obtained by truncating the distribution at finite minimum and maximum lengths, representing the shortest and longest rods in the sample.[49] The value of c_{iso} is insensitive to the minimum cutoff length in a reasonable range but quite sensitive to the maximum cutoff length. We define a dimensionless maximum cutoff length $l_{max} = L_{max}/L_0$. Wensink and Vroege compute c_{iso} for $l_{max} = 10$ and $l_{max} = 100$. While the value of l_{max} is not generally known for a given CNT sample, CNTs with $l_{max} > 20$ have been identified via near-infrared microscopy.[50] Therefore, we use the estimate $l_{max} = 100$ for evaluating the dependence of c_{iso} on φ_{iso} for CNT length distributions.

Combining eqs 14−16 and eqs 19−21 yields a system of 6 equations in 6 unknowns. To simplify integration, we define L_0 in terms of m and S

$$L_0 = e^{m+S^2} \quad (22)$$

Integrating eqs 14−16 from $L_{min} = 0.01L_0$ to $L_{max} = 100L_0$ and determining c_{iso} from Wensink and Vroege's isotropic cloud point data for a log-normal length distribution[49] (see Figure S2), we solve the system of eqs 14−16 and eqs 19−21 numerically and obtain the values of the m and S parameters as well as all moments of the length distribution. We can then compare length distributions of CNT samples determined by our method to CNT length distributions determined by other length measurement techniques.

EXPERIMENTAL METHODS

High-purity single-walled (SWNT) and double-walled (DWNT) carbon nanotubes were obtained from different manufacturers: high pressure carbon monoxide (HiPco) reactor at Rice University, UniDym Inc., Continental Carbon Nanotechnologies Inc. (CCNI), SouthWest NanoTechnologies Inc. (SWeNT), Meijo Nano Carbon Co. Ltd., Samsung Cheil Industries Inc., Teijin Aramid BV (TABV), and Linde Electronics. Raman spectra were acquired with a Renishaw InVia Confocal Raman microscope at 514, 633, and 785 nm excitation wavelengths. The spectra showed that all the CNT samples had relatively few defects (Raman G/D ratio at 633 nm >10). CNT diameters were measured from high-resolution TEM images of CNT samples taken with a JEOL 2010 TEM. Precise external wall boundaries were determined with ImageJ software.

CNTs were mixed with chlorosulfonic acid at concentrations in the range of 0.003% (30 ppm) to 0.5% (5000 ppm) by volume. CNT mass was measured on a mass balance, and chlorosulfonic acid volume was measured with a graduated cylinder. CNT mass fraction in acid was converted to volume fraction by multiplying the mass fraction M of CNTs in solution by the ratio of the solvent density ρ_s to the individual CNT density ρ_{CNT}

$$\varphi = M\frac{\rho_s}{\rho_{CNT}} \quad (23)$$

We use the individual CNT density rather than the density for hexagonally close-packed CNTs because the CNTs dissolve as individuals in chlorosulfonic acid. Accounting for the contribution of electron density to the external CNT diameter d gives the appropriate expression for CNT density[51]

$$\rho_{CNT} = \frac{4000}{A_S(d + \delta_{vdW})^2}\left[nd - 2\delta_{vdW}\sum_{i=0}^{n-1} i\right] \quad (24)$$

where $A_S = 1315$ m^2/g is the specific surface area for one side of a graphene sheet, n is the number of walls in the CNT, and $\delta_{vdW} = 0.34$ nm is the interlayer distance between two CNT walls. The CNTs were mixed in glass vials sealed with PTFE-lined silicone caps to prevent degradation of the cap by acid vapor. All solutions were speedmixed (FlackTek, Inc. DAC 150.1 speedmixer) for 10 min at 3500 rpm followed by 12 h of mixing with a magnetic stir bar on a Fischer Scientific stir plate.

The surface tension of pure chlorosulfonic acid with nitrogen was measured by the pendant drop method (CAM 2000 software) in a nitrogen environment, resulting in a value of $\gamma = 38$ mN/m. The shear viscosity of chlorosulfonic acid at 25 °C was measured at a shear rate of 10 s^{-1} with a TA Instruments AR 2000 rheometer enclosed in a drybox purged with dry air, resulting in a value of $\mu = 2.8$ mPa·s, consistent with literature values.[52]

Extensional viscosity of CNT solutions was measured with a Trimaster capillary thinning rheometer,[53] custom designed and built at Cambridge University. The rheometer consists of two pistons (1.2 mm diameter) that are moved apart axially from an initial separation of 0.6 mm. A stainless steel spatula was used to uniformly load solutions between the two pistons. The stretching rate was 25 mm/s (each piston moves at 12.5 mm/s), and the stretching distance was 1.0 mm for all samples. A Fastec Troubleshooter HR high-speed camera (1000 frames/s) was used to record videos of the capillary thinning tests. The filament profile was analyzed with Matlab software to determine the midplane diameter of the thinning fluid filament as a function of time. Because of the hygroscopic nature of chlorosulfonic acid, sample preparation and filament stretching were performed in a drybox continuously purged with dry air to keep the relative humidity level below 10%.

DOI: 10.1021/acs.macromol.5b02054
Macromolecules 2016, 49, 681−689

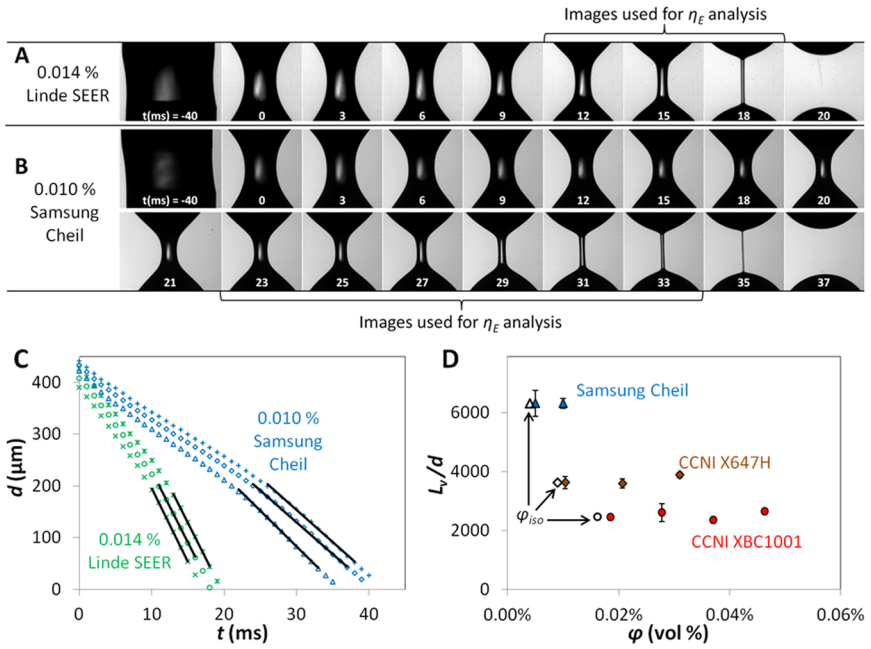

Figure 2. Filament profiles from capillary thinning experiments for (A) 0.014% Linde SEER and (B) 0.010% Samsung Cheil CNTs. (C) Plots of diameter evolution with time for both the Linde SEER and Samsung Cheil CNT solutions. Linear fits are shown for the portion of the filament thinning curves used to evaluate η_E. (D) Plot of L_v/d vs φ for Samsung Cheil, CCNI X647H, and CCNI XBC1001. Empty black symbols indicate the experimentally measured φ_{iso} for each sample.

To determine the isotropic cloud point, CNT solutions were flame-sealed in square capillaries from VitroTubes (0.1 mm height, 1 mm width) and observed with a polarized microscope (Zeiss Axioplan optical light microscope), as in earlier work on aqueous oxidized CNTs.[54] CNTs are known to form nematic liquid crystalline phases in chlorosulfonic acid,[17,31] enabling the detection of the isotropic cloud point by optical birefringence measurements on a series of CNT solutions. Solutions were initially prepared at concentrations above the isotropic cloud point (typically ~0.1 vol %) and then diluted until birefringence was no longer visible, indicating that the CNTs in solution had transitioned from a mixture of isotropic and nematic phases to a single isotropic phase.

Direct cryo-TEM imaging to measure CNT length was performed with a FEI T12 G^2 transmission electron microscope. Cryo-TEM samples were prepared with the procedure described by Davis et al.,[17] and CNT length was measured by tracing the end-to-end distance of individual CNTs in the TEM images as described by Behabtu et al.[9] We used this method to determine length with cryo-TEM in lieu of a faster, recently developed statistical method[21] because the statistical method only gives the average CNT length $\langle L \rangle$, whereas the tracing method yields the CNT length distribution.

RESULTS AND DISCUSSION

Extensional flows orient rigid molecules much more efficiently than shear flows. In shear flows, the vorticity always rotates the fluid's microstructure away from the principal axes of stretching. Therefore, the alignment of suspended particles under shear flow scales linearly with strain and time. Because of the irrotational nature of extensional flow, rod alignment can be reached at much smaller strain and time.[37] Processes such as fiber spinning take advantage of strong extensional flows to align rodlike molecules in solution prior to removing the solvent and solidifying the fibers. Similarly, we capitalize on the ability of extensional flows to ensure complete alignment of CNTs in solutions that have been stretched to form unstable filaments, prior to observing the capillary breakup of the filaments.

Extensional Viscosity. Filament profiles from capillary thinning experiments of CNT solutions made with Linde SEER and Samsung Cheil CNTs are displayed in Figure 2A,B. The filament profiles give no indication of fluid inhomogeneities, and all the profiles are symmetric about the midfilament. Time is measured starting when the pistons stop moving (t = 0). Figure 2C shows that initially D_{mid} decreases linearly with time, but the slope changes during the later stages of necking for both CNT samples. The linear decrease in diameter during the later stages is Newtonian-like behavior (i.e., the viscosity does not change with strain), indicating that the CNTs in solution are not experiencing (volume averaged) orientational changes during that period. We calculate η_E using the thinning rate dD_{mid}/dt during the later stages of necking because the assumption of a slender filament with negligible gravity, inertia, and axial curvature is only appropriate in the thinning regime closest to filament breakup.[38]

The fits to the diameter evolution curves used to determine η_E for Linde SEER and Samsung Cheil CNT solutions are shown in Figure 2C, and the filament profile images corresponding to the fits are highlighted in Figure 2A,B. Figure 2D shows that the measured aspect ratios are independent of concentration (for solutions with breakup times <50 ms) even when some nematic phase is present, as long as $\varphi < 3\ \varphi_{iso}$. In principle, the model used to relate extensional viscosity to length requires that the CNTs should be in the isotropic phase; however, the viscosity of isotropic CNT solutions was too low for self-thinning fluid filaments to form. Therefore, CNTs were mixed at concentrations slightly above φ_{iso}, resulting in filament breakup times between 10 and 50 ms after the cessation of piston motion. Solutions with breakup times greater than 50 ms were not used for calculating aspect ratio because they exhibited thinning dynamics inconsistent with Newtonian dynamics. Although some amount of nematic phase is present in the CNT samples used in capillary thinning experiments, we

DOI: 10.1021/acs.macromol.5b02054
Macromolecules 2016, 49, 681−689

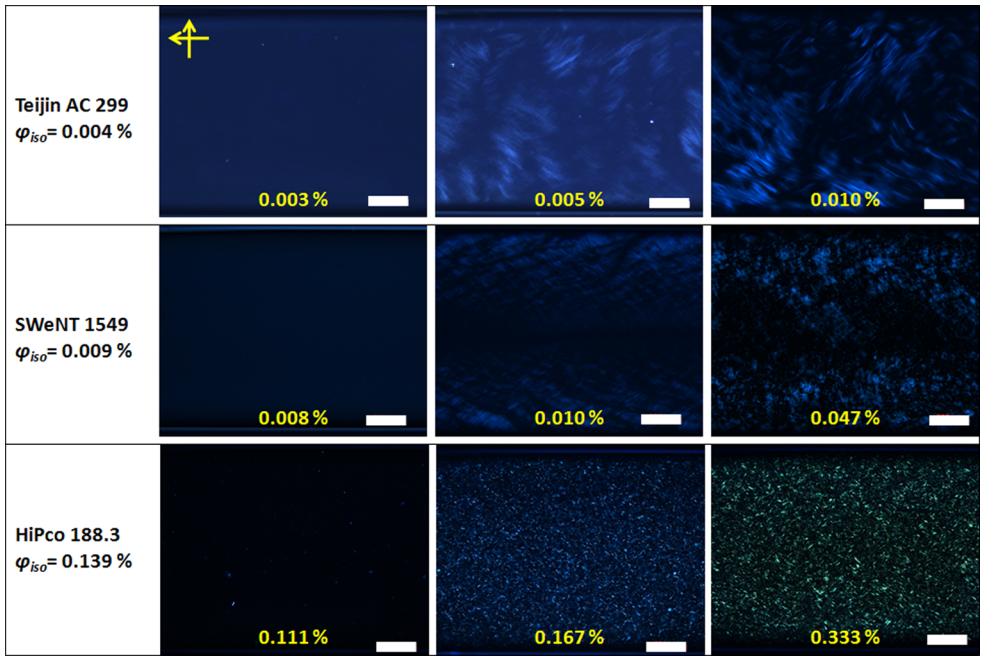

Figure 3. Polarized light microscopy images for the determination of φ_{iso} for Teijin AC 299, SWeNT PXD1-1549, and HiPco 188.3 CNTs. The arrows at the top left indicate the relative orientation of the polarizer to the analyzer for all of the above images. Scale bars are 200 μm.

find that the presence of such a small amount of nematic phase does not appear to affect the estimation of CNT aspect ratio through extensional viscosity measurements. This behavior is not unexpected because CNTs flow-align under extensional flow, and hence the nematic and isotropic phases merge into a single aligned phase during capillary thinning.

A high degree of CNT alignment in the stretching direction during capillary thinning is necessary to extract CNT aspect ratios from extensional viscosity measurements. Increasing strain during self-thinning should result in strain hardening (i.e., increasing extensional viscosity) if the degree of CNT alignment is still changing after the relatively high initial strain rate (100 s^{-1}) imposed on the CNT solution during the initial stretching by the rheometer pistons. The absence of strain hardening throughout self-thinning implies that the average orientation of CNTs does not change after the initial step strain, but this does not prove that the CNTs are fully aligned during capillary thinning.

However, previously reported capillary thinning experiments on CNT dispersions in epoxy indicated that 97−99% of CNTs were aligned in the stretching direction immediately after the initial step strain was imposed by the rheometer.[33] Moreover, extensional viscosity measurements performed with a filament stretching extensional rheometer (FiSER) on surfactant stabilized HiPco SWNT dispersions suggest that imposing a Hencky strain of ∼1 is sufficient to fully align CNTs in solution.[55] Hencky strain ε is given by

$$\varepsilon = 2 \ln\left(\frac{D_{0,\mathrm{mid}}}{D_{\mathrm{mid}}}\right) \tag{25}$$

where $D_{0,\mathrm{mid}}$ is the initial diameter of the fluid filament before stretching. When Hencky strain exceeded 1, Nguyen et al. observed an extensional viscosity plateau, along with no evidence of extension rate dependence; both were strong indications that CNTs had become completely aligned in their solutions. Therefore, extensional viscosity from capillary thinning experiments in this work is only calculated at Hencky strains above 1, when the CNTs in the acid solutions are expected to be fully aligned and the solutions have the flow-independent (Newtonian-like) extensional viscosity shown in the high extension rate plateau region of Figure 1.

Isotropic Cloud Point. We measure φ_{iso} for each CNT sample to assess how CNT aspect ratio and length polydispersity affect CNT liquid crystalline phase behavior. Figure 3 shows cross-polarized light microscopy images of CNT solutions in flame-sealed capillaries ranging from φ = 0.003% (30 ppm) to φ = 0.333% (3330 ppm) for three different CNT samples. Isotropic CNT solutions appear dark, while solutions containing a nematic liquid crystalline phase are birefringent. We define φ_{iso} as the concentration at the midpoint between the most concentrated not birefringent solution and the least concentrated birefringent solution. TABV AC 299 CNTs had the lowest value of φ_{iso} of any of the tested samples (0.004%); this value is more than 1 order of magnitude lower than φ_{iso} of f-actin solutions[56] (∼0.1%), and it is significantly lower than previously reported values of φ_{iso} of CNT liquid crystalline solutions[57] (∼0.007%). The extremely low φ_{iso} values for some of our CNT samples are indicative of the high aspect ratios of the CNTs as well as of the presence of polydispersity in the samples.

Onsager's theory[16] predicts that in solutions of monodisperse rigid rods, $\varphi_{iso} = 3.34(L/d)^{-1}$. According to theory,[49] the scaling of $\varphi_{iso} \sim (L/d)^{-1}$ should still hold for samples of polydisperse rods, as long as the rods' polydispersities are comparable. We characterize the length polydispersity of CNT samples later in this report. Figure 4 shows that φ_{iso} of CNT samples indeed follows Onsager scaling (best fit exponent $(L_v/d)^{-1.07}$), while length polydispersity lowers φ_{iso} by an order of magnitude compared to Onsager's predicted isotropic cloud point $\varphi_{Onsager}$ for monodisperse rods with $L = L_v$. Length polydispersity leads to a decrease in φ_{iso} because the longest CNTs in solution preferentially form a nematic phase at lower concentrations than the shorter CNTs.[49] The excellent

DOI: 10.1021/acs.macromol.5b02054
Macromolecules 2016, 49, 681−689

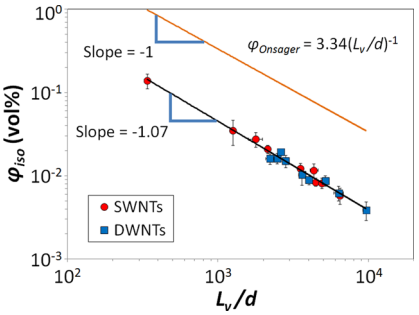

Figure 4. Isotropic cloud point as a function of CNT aspect ratio for all the SWNT (red) and DWNT (blue) samples tested in this work. The black line is a power law fit to the experimental data. The orange line shows Onsager's prediction for solutions of monodisperse rigid rods.[16]

agreement with Onsager's scaling provides a consistency check that L_v/d is indeed capturing the relative length of different CNT samples. Moreover, combining φ_{iso} with L_v/d provides an avenue for estimating the length distribution of the CNT samples.

Length Distribution Results. We calculate the m and S parameters as well as the moments of the length distribution for each CNT sample after determining L_v/d from extensional viscosity, d from TEM, and φ_{iso} from polarized light microscopy. We find that CNT samples ranged in length from L_v = 0.39 μm for HiPco 188.3 CNTs to L_v = 20.17 μm for Teijin AC 299 CNTs. Table 1 shows the aspect ratio, CNT solution concentration, extensional viscosity, diameter, viscosity average length, isotropic cloud point, polydispersity index, and average length of all tested CNT samples from various suppliers. The σ_L of the samples ranged from 1.19 to 1.69, which is higher than typical polydispersities for colloidal spheres ($1.0 < \sigma_L < 1.2$)[58] but surprisingly low by polymeric sample standards (typically polymeric samples are considered narrowly disperse when $\sigma_L \lesssim 2$). It is noteworthy that CNT growth methods that are quite different yield CNT samples with relatively comparable polydispersities. While the specific growth mechanism that determines CNT length polydispersity is unknown, the range of polydispersities observed in this work is consistent with polydispersities of CNT samples measured with direct imaging techniques[9,23,54] and suggests that termination of growth may have a strong degree of commonality across different reaction methods that include supported as well as unsupported catalyst.

In principle, the difference between measured φ_{iso} and $\varphi_{Onsager}$ should be greater for samples with higher σ_L. Figure 5

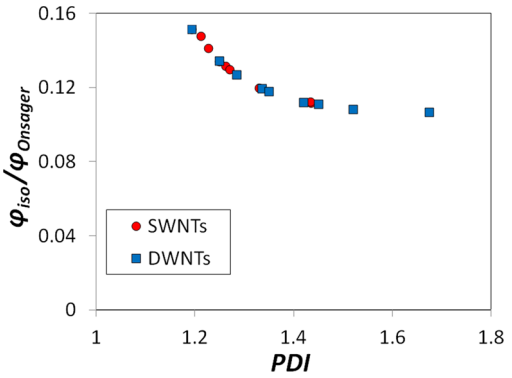

Figure 5. Ratio of φ_{iso} to $\varphi_{Onsager}$ as a function of σ_L for all the SWNT (red) and DWNT (blue) samples tested in this work.

confirms that this is indeed the case for the CNT samples tested in this study as it shows that the ratio of φ_{iso} to $\varphi_{Onsager}$ decreases for samples with higher σ_L. These results confirm the prediction that increasing σ_L will lower the isotropic cloud point of CNT solutions.[41] Therefore, we deem that σ_L values estimated from our inferred length distributions for the various CNT samples are reasonable.

Comparison to Cryo-TEM Length Measurements. To check the quantitative accuracy of our inferred CNT length distributions, we compare the relevant length moments from our inferred log-normal length distribution for CCNI XBC1001 to one measured directly by cryo-TEM imaging.[9,57] Cryo-TEM of CNT solutions in CSA is currently the only direct measurement technique that can measure CNT length distributions without sonication, thereby avoiding breaking of

Table 1. Length Distribution Data for CNT Samples from Different Manufacturers Listed in Descending Order of Aspect Ratio

sample	L_v/d	φ (ppm)	η_E (Pa·s)	d (nm)	L_v (μm)	φ_{iso} (ppm)	σ_L	$\langle L \rangle$ (μm)
TABV AC 299	9610 ± 470	49	1.36 ± 0.13	2.1 ± 0.7	20.17	39 ± 10	1.42	11.86
Meijo EC1.5	6430 ± 290	130	1.78 ± 0.16	1.5 ± 0.2	9.65	55 ± 10	1.69	4.41
Samsung Cheil	6310 ± 440	100	1.29 ± 0.07	2.2 ± 0.5	13.89	62 ± 12	1.35	8.87
Samsung 98P	5150 ± 130	100	0.86 ± 0.04	2.2 ± 0.5	11.32	87 ± 12	1.25	8.11
SWeNT 1555	4900 ± 260	117	0.93 ± 0.10	0.8 ± 0.1	3.92	82 ± 12	1.33	2.56
SWeNT 1549	4440 ± 310	93	0.60 ± 0.08	0.8 ± 0.1	3.55	84 ± 9	1.43	2.07
SWeNT 1167	4330 ± 270	140	0.88 ± 0.11	0.8 ± 0.1	3.46	117 ± 23	1.19	2.66
UniDym UA	4010 ± 80	146	0.79 ± 0.03	2.1 ± 0.6	7.81	90 ± 12	1.52	4.50
CCNI X647H	3600 ± 160	207	0.93 ± 0.08	2.3 ± 0.5	8.41	103 ± 26	1.45	4.82
Linde SEER	3520 ± 20	141	0.59 ± 0.01	1.7 ± 0.3	5.98	123 ± 18	1.27	4.18
CCNI XBC1101	2810 ± 60	378	1.11 ± 0.04	3.2 ± 1.0	8.98	151 ± 25	1.28	6.17
CCNI X647H3	2610 ± 90	207	0.50 ± 0.04	2.3 ± 0.5	6.11	194 ± 13	1.19	4.69
CCNI XBC1001	2470 ± 30	190	0.39 ± 0.01	1.9 ± 0.6	4.68	162 ± 23	1.34	3.03
UniDym OE	2210 ± 80	461	0.86 ± 0.11	1.9 ± 0.6	4.16	161 ± 23	1.67	1.92
SWeNT 1392	2130 ± 50	467	0.81 ± 0.04	0.8 ± 0.1	1.71	210 ± 23	1.25	1.23
HiPco 183.6	1780 ± 190	555	0.69 ± 0.14	1.1 ± 0.2	2.04	280 ± 60	1.21	1.51
SWeNT CG300	1250 ± 60	467	0.29 ± 0.03	0.8 ± 0.1	1.00	350 ± 120	1.26	0.71
HiPco 188.3	340 ± 10	5000	0.31 ± 0.02	1.1 ± 0.2	0.39	1390 ± 280	1.23	0.29

DOI: 10.1021/acs.macromol.5b02054
Macromolecules 2016, 49, 681−689

CNTs. A total of 23 individual CCNI XBC1001 CNTs were measured with direct cryo-TEM imaging by tracing the entire length of each CNT. Figure 6 shows that the probability density

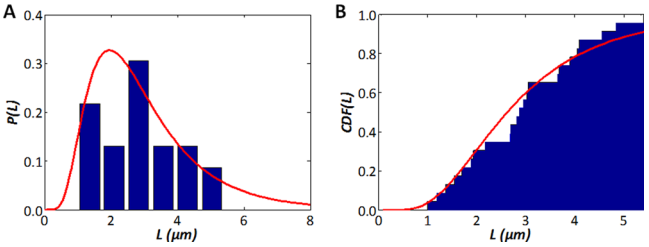

Figure 6. (A) Probability density function and (B) cumulative distribution function for length data from the L_v/d and φ_{iso} measurements (solid red line) and from direct cryo-TEM imaging (blue bars) of 23 individual CCNI XBC1001 CNTs.

function and cumulative distribution function of the cryo-TEM data agree well with the distribution that we calculate from our measurements of L_v/d and φ_{iso}. The average length measured by cryo-TEM for CCNI XBC1001, $\langle L \rangle = 2.91$ μm, is within 4% of the value calculated from L_v/d and φ_{iso} measurements, $\langle L \rangle = 3.03$ μm. The close agreement between the inferred length distribution and the distribution measured by cryo-TEM validates the accuracy of length distributions inferred from L_v/d and φ_{iso} measurements. Moreover, measuring L_v/d and φ_{iso} is significantly faster than using the direct imaging cryo-TEM method to characterize a CNT length distribution. In addition, direct imaging of CNTs longer than ~5 μm can result in underestimation of the average CNT length because it is difficult to follow CNTs longer than 5 μm from end to end—these issues can be partially circumvented by applying a statistical method.[21]

CONCLUSIONS

This study shows that average CNT aspect ratio can be accurately determined from capillary thinning extensional viscosity measurements of semidilute CNT solutions in chlorosulfonic acid by applying Shaqfeh and Fredrickson's equation for semidilute suspensions of rigid rods.[40] The method is applicable to CNT dispersions in other solvents as long as CNTs are dispersed as individuals. Determining the aspect ratio from extensional viscosity measurements is faster and more reliable than cryo-TEM, and it also circumvents the issues that plague AFM, such as small sample size, use of sonication, and a bias toward measuring longer CNTs. Most importantly, the extensional viscosity technique makes it possible to accurately measure aspect ratio for CNTs over a wider range of lengths than previously possible (few hundred nanometers to tens of micrometers). Optical birefringence measurements of the isotropic cloud point for the highest aspect ratio CNT sample result in an isotropic cloud point of ~40 ppm, an astonishingly low concentration that is well below published experimental results for liquid crystalline solutions of rodlike molecules. Manufacturers of CNTs without access to an extensional rheometer could use isotropic cloud point measurements as a simple length indexing method for comparing different batches of CNTs. Coupled with the aspect ratio and TEM diameter measurements, the isotropic cloud point measurements are used to determine the parameters of each CNT sample's length distribution. The dependence of the isotropic cloud point on CNT aspect ratio is consistent with Onsager-like scaling due to the relatively narrow range of length polydispersities across the CNT samples. Because properties of CNT materials are highly dependent on the length of constituent CNTs, the ability to accurately measure length distributions for very long CNTs is critical for developing superior CNT fibers and films.

ASSOCIATED CONTENT

Supporting Information

The Supporting Information is available free of charge on the ACS Publications website at DOI: 10.1021/acs.macromol.5b02054.

Text S1, maximum rod length measurable with shear rheology; text S2, isotropic cloud point vs polydispersity (PDF)

AUTHOR INFORMATION

Corresponding Author

*E-mail: mp@rice.edu (M.P.).

Author Contributions

D.E.T., A.C., J.H., Y.L., and E.A.B. performed experimental work. N.B., A.W.K.M., and D.E.T. designed and set up experimental equipment. D.E.T., J.A.L., R.J.H., M.J.G., and Y.T. analyzed experimental results and verified the theoretical basis of the research. D.E.T., A.W.K.M., and M.P. conceived and designed the research, and M.P. directed the research. D.E.T. and M.P wrote the manuscript with input from all coauthors.

Notes

The authors declare no competing financial interest.

ACKNOWLEDGMENTS

We thank S. Fogden, K. Takano, M. Otto, K. McElrath, E. Vega, X. Hu, G. Irvin, Y. Tan, and L. Ci for providing CNTs; C. Young, B. Whiting, and M. Mackley for useful discussions; and O. Kleinerman, E. Kesselman, and J. Schmidt for providing cryo-TEM images, collected at the Technion Laboratory for Electron Microscopy of Soft Matter, supported by the Technion Russell Berrie Nanotechnology Institute (RBNI). This work was supported by Teijin Aramid BV, Teijin Techno Products Ltd., the Welch Foundation (C-1668 and Evans Attwell fellowship), the United States−Israel Binational Science Foundation (BSF), Air Force Office of Scientific Research FA9550-09-1-0590 and FA9550-15-1-0370 and MURI grant FA9550-12-1-0035, and NSF NSEC Center for Hierarchical Manufacturing (CMMI-0531171 and CMMI-1031171). R.J.H. was supported by a NASA Space Technology Research Fellowship Grant NNX14AL71H.

REFERENCES

(1) Green, M. J.; Behabtu, N.; Pasquali, M.; Adams, W. W. *Polymer* **2009**, *50*, 4979−4997.
(2) Hone, J.; Llaguno, M. C.; Nemes, N. M.; Johnson, A. T.; Fischer, J. E.; Walters, D. A.; Casavant, M. J.; Schmidt, J.; Smalley, R. E. *Appl. Phys. Lett.* **2000**, *77*, 666−668.
(3) Liew, K. M.; He, X. Q.; Wong, C. H. *Acta Mater.* **2004**, *52*, 2521−2527.
(4) Baughman, R. H.; Zakhidov, A. A.; de Heer, W. A. *Science* **2002**, *297*, 787−792.
(5) Mirri, F.; Ma, A. W. K.; Hsu, T. T.; Behabtu, N.; Eichmann, S. L.; Young, C. C.; Tsentalovich, D. E.; Pasquali, M. *ACS Nano* **2012**, *6*, 9737−9744.

DOI: 10.1021/acs.macromol.5b02054
Macromolecules 2016, 49, 681−689

(6) Wu, Z. C.; Chen, Z. H.; Du, X.; Logan, J. M.; Sippel, J.; Nikolou, M.; Kamaras, K.; Reynolds, J. R.; Tanner, D. B.; Hebard, A. F.; Rinzler, A. G. *Science* **2004**, *305*, 1273−1276.
(7) Sierros, K. A.; Hecht, D. S.; Banerjee, D. A.; Morris, N. J.; Hu, L.; Irvin, G. C.; Lee, R. S.; Cairns, D. R. *Thin Solid Films* **2010**, *518*, 6977−6983.
(8) Zakhidov, A. A.; Nanjundaswamy, R.; Obraztsov, A. N.; Zhang, M.; Fang, S.; Klesch, V. I.; Baughman, R. H.; Zakhidov, A. A. *Appl. Phys. A: Mater. Sci. Process.* **2007**, *88*, 593−600.
(9) Behabtu, N.; Young, C. C.; Tsentalovich, D. E.; Kleinerman, O.; Wang, X.; Ma, A. W. K.; Bengio, E. A.; ter Waarbeek, R. F.; de Jong, J. J.; Hoogerwerf, R. E.; Fairchild, S. B.; Ferguson, J. B.; Maruyama, B.; Kono, J.; Talmon, Y.; Cohen, Y.; Otto, M. J.; Pasquali, M. *Science* **2013**, *339*, 182−186.
(10) Park, S.; Vosguerichian, M.; Bao, Z. *Nanoscale* **2013**, *5*, 1727−1752.
(11) Jarosz, P.; Schauerman, C.; Alvarenga, J.; Moses, B.; Mastrangelo, T.; Raffaelle, R.; Ridgley, R.; Landi, B. *Nanoscale* **2011**, *3*, 4542−4553.
(12) Zhang, X.; Li, Q.; Tu, Y.; Li, Y.; Coulter, J. Y.; Zheng, L.; Zhao, Y.; Jia, Q.; Peterson, D. E.; Zhu, Y. *Small* **2007**, *3*, 244−248.
(13) Yakobson, B. I.; Samsonidze, G.; Samsonidze, G. G. *Carbon* **2000**, *38*, 1675−1680.
(14) Behabtu, N.; Green, M. J.; Pasquali, M. *Nano Today* **2008**, *3*, 24−34.
(15) Hecht, D. S.; Hu, L.; Gruner, G. *Curr. Appl. Phys.* **2007**, *7*, 60−63.
(16) Onsager, L. *Ann. N. Y. Acad. Sci.* **1949**, *51*, 627−659.
(17) Davis, V. A.; Parra-Vasquez, A. N. G.; Green, M. J.; Rai, P. K.; Behabtu, N.; Prieto, V.; Booker, R. D.; Schmidt, J.; Kesselman, E.; Zhou, W.; Fan, H.; Adams, W. W.; Hauge, R. H.; Fischer, J. E.; Cohen, Y.; Talmon, Y.; Smalley, R. E.; Pasquali, M. *Nat. Nanotechnol.* **2009**, *4*, 830−834.
(18) Fagan, J. A.; Bauer, B. J.; Hobbie, E. K.; Becker, M. L.; Walker, A. R. H.; Simpson, J. R.; Chun, J.; Obrzut, J.; Bajpai, V.; Phelan, F. R.; Simien, D.; Huh, J. Y.; Migler, K. B. *Adv. Mater.* **2011**, *23*, 338−348.
(19) Islam, M. F.; Rojas, E.; Bergey, D. M.; Johnson, A. T.; Yodh, A. G. *Nano Lett.* **2003**, *3*, 269−273.
(20) Ziegler, K. J.; Gu, Z. N.; Shaver, J.; Chen, Z. Y.; Flor, E. L.; Schmidt, D. J.; Chan, C.; Hauge, R. H.; Smalley, R. E. *Nanotechnology* **2005**, *16*, S539−S544.
(21) Bengio, E. A.; Tsentalovich, D. E.; Behabtu, N.; Kleinerman, O.; Kesselman, E.; Schmidt, J.; Talmon, Y.; Pasquali, M. *ACS Appl. Mater. Interfaces* **2014**, *6*, 6139−6146.
(22) Badaire, S.; Poulin, P.; Maugey, M.; Zakri, C. *Langmuir* **2004**, *20*, 10367−10370.
(23) Streit, J. K.; Bachilo, S. M.; Naumov, A. V.; Khripin, C.; Zheng, M.; Weisman, R. B. *ACS Nano* **2012**, *6*, 8424−8431.
(24) Mayne, M.; Grobert, N.; Terrones, M.; Kamalakaran, R.; Ruhle, M.; Kroto, H. W.; Walton, D. R. M. *Chem. Phys. Lett.* **2001**, *338*, 101−107.
(25) Parra-Vasquez, A. N. G.; Stepanek, I.; Davis, V. A.; Moore, V. C.; Haroz, E. H.; Shaver, J.; Hauge, R. H.; Smalley, R. E.; Pasquali, M. *Macromolecules* **2007**, *40*, 4043−4047.
(26) Bengio, E. A.; Tsentalovich, D. E.; Behabtu, N.; Kleinerman, O.; Kesselman, E.; Schmidt, J.; Talmon, Y.; Pasquali, M. *ACS Appl. Mater. Interfaces* **2014**, *6*, 6139.
(27) Hennrich, F.; Krupke, R.; Arnold, K.; Stuetz, J. A. R.; Lebedkin, S.; Koch, T.; Schimmel, T.; Kappes, M. M. *J. Phys. Chem. B* **2007**, *111*, 1932−1937.
(28) Pagani, G.; Green, M. J.; Poulin, P.; Pasquali, M. *Proc. Natl. Acad. Sci. U. S. A.* **2012**, *109*, 11599−11604.
(29) Lucas, A.; Zakri, C.; Maugey, M.; Pasquali, M.; van der Schoot, P.; Poulin, P. *J. Phys. Chem. C* **2009**, *113*, 20599−20605.
(30) Parra-Vasquez, A. N. G. Doctoral Thesis, Rice University, 2009.
(31) Davis, V. A.; Ericson, L. M.; Parra-Vasquez, A. N. G.; Fan, H.; Wang, Y. H.; Prieto, V.; Longoria, J. A.; Ramesh, S.; Saini, R. K.; Kittrell, C.; Billups, W. E.; Adams, W. W.; Hauge, R. H.; Smalley, R. E.; Pasquali, M. *Macromolecules* **2004**, *37*, 154−160.
(32) Duggal, R.; Pasquali, M. *Phys. Rev. Lett.* **2006**, *96*, 246104.
(33) Ma, A. W. K.; Chinesta, F.; Tuladhar, T.; Mackley, M. R. *Rheol. Acta* **2008**, *47*, 447−457.
(34) Tiwari, M. K.; Bazilevsky, A. V.; Yarin, A. L.; Megaridis, C. M. *Rheol. Acta* **2009**, *48*, 597−609.
(35) Ramesh, S.; Ericson, L. M.; Davis, V. A.; Saini, R. K.; Kittrell, C.; Pasquali, M.; Billups, W. E.; Adams, W. W.; Hauge, R. H.; Smalley, R. E. *J. Phys. Chem. B* **2004**, *108*, 8794−8798.
(36) Bhat, P. P.; Appathurai, S.; Harris, M. T.; Pasquali, M.; McKinley, G. H.; Basaran, O. A. *Nat. Phys.* **2010**, *6*, 625−631.
(37) McKinley, G. H.; Sridhar, T. *Annu. Rev. Fluid Mech.* **2002**, *34*, 375−415.
(38) McKinley, G. H.; Tripathi, A. *J. Rheol.* **2000**, *44*, 653−670.
(39) Batchelor, G. K. *J. Fluid Mech.* **1971**, *46*, 813−829.
(40) Shaqfeh, E. S. G.; Fredrickson, G. H. *Phys. Fluids A* **1990**, *2*, 7−24.
(41) Green, M. J.; Parra-Vasquez, A. N. G.; Behabtu, N.; Pasquali, M. *J. Chem. Phys.* **2009**, *131*, 084901.
(42) Bazilevsky, A. V.; Entov, V. M.; Rozhkov, A. N. In *Third European Rheology Conference*; Oliver, D. R., Ed.; Elsevier: New York, 1990.
(43) Entov, V. M.; Hinch, E. J. *J. Non-Newtonian Fluid Mech.* **1997**, *72*, 31−53.
(44) Tuladhar, T. R.; Mackley, M. R. *J. Non-Newtonian Fluid Mech.* **2008**, *148*, 97−108.
(45) Papageorgiou, D. T. *Phys. Fluids* **1995**, *7*, 1529−1544.
(46) Larson, R. G. *The Structure and Rheology of Complex Fluids*; Oxford University Press: New York, 1999.
(47) Batchelor, G. K. *J. Fluid Mech.* **1970**, *41*, 545−570.
(48) Ebdon, J. R. *Polym. Int.* **1992**, *27*, 207−208.
(49) Wensink, H. H.; Vroege, G. J. *J. Chem. Phys.* **2003**, *119*, 6868−6882.
(50) Fakhri, N.; MacKintosh, F. C.; Lounis, B.; Cognet, L.; Pasquali, M. *Science* **2010**, *330*, 1804−1807.
(51) Laurent, C.; Flahaut, E.; Peigney, A. *Carbon* **2010**, *48*, 2994−2996.
(52) Cremlyn, R. J. W.; Chemistry, R. S. O *Chlorosulfonic Acid: A Versatile Reagent*; Royal Society of Chemistry: 2002.
(53) Vadillo, D. C.; Tuladhar, T. R.; Mulji, A. C.; Jung, S.; Hoath, S. D.; Mackley, M. R. *J. Rheol.* **2010**, *54*, 261−282.
(54) Song, W. H.; Windle, A. H. *Macromolecules* **2005**, *38*, 6181−6188.
(55) Nguyen, D. A.; Dan, B.; Parra-Vasquez, A. N. G.; Pasquali, M.; Prakash, J. R.; Sridhar, T. Paper presented at the International Congress on Rheology, Monterey, CA, 2008.
(56) Viamontes, J.; Tang, J. X. *Phys. Rev. E:* **2003**, *67*, 040701.
(57) Parra-Vasquez, A. N. G.; Behabtu, N.; Green, M. J.; Pint, C. L.; Young, C. C.; Schmidt, J.; Kesselman, E.; Goyal, A.; Ajayan, P. M.; Cohen, Y.; Talmon, Y.; Hauge, R. H.; Pasquali, M. *ACS Nano* **2010**, *4*, 3969−3978.
(58) Desmond, K. W.; Weeks, E. R. *Phys. Rev. E* **2014**, *90*, 022204.

DOI: 10.1021/acs.macromol.5b02054
Macromolecules 2016, 49, 681−689